Molecular-receptor-specific, non-toxic, near-infrared-emitting Au cluster-protein nanoconjugates for targeted cancer imaging

2010 Nanotechnology 21 055103

(http://iopscience.iop.org/0957-4484/21/5/055103)

Nanotechnology **21** (2010) 055103 (12pp) doi:10.1088/0957-4484/21/5/055103

Molecular-receptor-specific, non-toxic, near-infrared-emitting Au cluster-protein nanoconjugates for targeted cancer imaging

Archana Retnakumari[1], Sonali Setua[1], Deepthy Menon[1], Prasanth Ravindran[1], Habeeb Muhammed[2], Thalappil Pradeep[2], Shantikumar Nair[1] and Manzoor Koyakutty[1,3]

[1] Amrita Centre for Nanoscience and Molecular Medicine, Amrita Institute of Medical Science, Cochin, 682 041, India
[2] Indian Institute of Technology, DST unit on Nanoscience, Chennai, 600 036, India

E-mail: manzoor_nanomed@yahoo.com

Received 24 September 2009, in final form 21 November 2009
Published 21 December 2009
Online at stacks.iop.org/Nano/21/055103

Abstract

Molecular-receptor-targeted imaging of folate receptor positive oral carcinoma cells using folic-acid-conjugated fluorescent Au_{25} nanoclusters (Au NCs) is reported. Highly fluorescent Au_{25} clusters were synthesized by controlled reduction of Au^{+} ions, stabilized in bovine serum albumin (BSA), using a green-chemical reducing agent, ascorbic acid (vitamin-C). For targeted-imaging-based detection of cancer cells, the clusters were conjugated with folic acid (FA) through amide linkage with the BSA shell. The bioconjugated clusters show excellent stability over a wide range of pH from 4 to 14 and fluorescence efficiency of ∼5.7% at pH 7.4 in phosphate buffer saline (PBS), indicating effective protection of nanoclusters by serum albumin during the bioconjugation reaction and cell–cluster interaction. The nanoclusters were characterized for their physico-chemical properties, toxicity and cancer targeting efficacy *in vitro*. X-ray photoelectron spectroscopy (XPS) suggests binding energies correlating to metal Au $4f_{7/2}$ ∼ 83.97 eV and Au $4f_{5/2}$ ∼ 87.768 eV. Transmission electron microscopy and atomic force microscopy revealed the formation of individual nanoclusters of size ∼1 nm and protein cluster aggregates of size ∼8 nm. Photoluminescence studies show bright fluorescence with peak maximum at ∼674 nm with the spectral profile covering the near-infrared (NIR) region, making it possible to image clusters at the 700–800 nm emission window where the tissue absorption of light is minimum. The cell viability and reactive oxygen toxicity studies indicate the non-toxic nature of the Au clusters up to relatively higher concentrations of 500 μg ml^{-1}. Receptor-targeted cancer detection using Au clusters is demonstrated on FR^{+ve} oral squamous cell carcinoma (KB) and breast adenocarcinoma cell MCF-7, where the FA-conjugated Au_{25} clusters were found internalized in significantly higher concentrations compared to the negative control cell lines. This study demonstrates the potential of using non-toxic fluorescent Au nanoclusters for the targeted imaging of cancer.

(Some figures in this article are in colour only in the electronic version)

1. Introduction

Targeted imaging of cancer by simple yet high-resolution optical and chemical methods has gathered momentum in recent times [1, 2]. Fluorescent quantum dot (QD)-based optical imaging of cells has been a focus of researchers during the past few years, owing to their unique optical, electronic and physico-chemical characteristics [3, 4]. Although QDs have numerous advantages over conventional organic dyes

[3] Author to whom any correspondence should be addressed.

and fluorescent proteins such as intense luminescence, high molar extinction coefficient, resistance to photo-bleaching and broad excitation with narrow emission bands ideal for high contrast optical imaging of biological systems [5] the inherent compositional toxicity prevailing in most of the QDs limit their practical application potential, particularly in clinical scenarios [6]. In this context, it is important to develop alternative biocompatible luminescent non-toxic nanobioprobes for high contrast optical imaging.

Molecular clusters of plasmonic nanocrystals, particularly gold (Au) and silver (Ag), are a new class of colloidal fluorescent clusters that can find possible applications in medical imaging [7]. Compared to large-sized nanoparticles (10–100 nm) Au clusters consisting of a magic number of atoms (Au_n, where $n = 18$, 21, 25, 28, 32 or 39), show no surface plasmon resonance but exhibit vis–NIR fluorescence owing to the formation of molecular-type HOMO–LUMO bandgap opening as well as electronic transitions at sub-nanometer sizes smaller than the Fermi wavelength (i.e. <1 nm) [8]. Optical absorption spectroscopy of Au_{28} clusters with core diameters of $\sim$0.9 nm show an energy bandgap of $\sim$1.3 eV, which is much higher than the average energy of bulk phonons, $\sim$10 mV, and therefore radiative recombination of e–h pairs is competent with photon-assisted non-radiative relaxation. However, due to the stringent size sensitivity of such quantum mechanical properties, it was relatively difficult to synthesize and stabilize atomic clusters, particularly for their use in practical applications. From various processing methods reported, a versatile synthetic strategy adopted by many groups is based on thiol-protected synthesis or 'ligand-etching' of pre-formed larger nanoparticles or clusters into sub-nanometer clusters. Among several ligand-etched systems, glutathiolated (GSH) Au clusters $(Au)_n(SG)_m$ remain one of the most elegant cluster systems owing to their high stability as well as their well-defined size [9].

While considering the practical applications of fluorescent metal clusters for biomedical imaging, there are a number of challenges that remain to be resolved: (a) very low fluorescence quantum efficiency of thiol-protected clusters, of the order of $\sim 10^{-3}$–10^{-5}, which is practically insignificant compared to fluorescent dyes or QDs [7], (b) the monolayer of the GSH tri-peptide ligand shell bonded to an Au core by Au–S linkage undergoes fast enzymatic degradation while interacting with cellular systems leading to loss of cluster identity and fluorescence, (c) the stability of monolayer-protected clusters and hence their fluorescence properties are sensitive to a wide range of pH conditions that are encountered during bioconjugation reaction protocols and interaction with cell membrane, endosomes or lysosomes [10], (d) stability of clusters being highly sensitive to the nature of the surface ligand (shell), any surface derivatization with biomolecules such as antibodies, peptides or small molecules may impair the fluorescence properties and (e) toxicity of metallic clusters and its associated ligands in biological systems is least evaluated [11]. In effect, the biomedical application of Au clusters demands a new set of experiments towards optimizing the above listed parameters of biological importance, apart from the challenges posed by its synthesis. In this direction, recently, Xie *et al* have reported an important alternative method of synthesizing fluorescent Au_{25} NCs ($\sim$0.8 nm) having a fluorescence QE of $\sim$6% using BSA as a reductant as well as a stabilizing agent [12]. Proteins like BSA are stable against biochemical degradation due to its rich and complex architecture constituted by repeated units of amino acids like cysteine, tyrosine and tryptophan [13]. Further, Lin *et al* have shown that fluorescent Au clusters can be used for optical imaging of cells [14].

In the current investigation, we show the possibility of using BSA-stabilized Au clusters for one of the most demanding requirements of oncology; 'single-cell-targeted imaging'-based cancer detection at an early stage. In this context, the challenges of using fluorescent metal nanoclusters for cancer imaging are twofold: (a) maintaining the fluorescence properties of ligand-sensitive clusters during the bioconjugation reaction involving different pH conditions and repeated purification steps and (b) the adverse effects of the protective ligand, namely BSA, towards competitive non-specific uptake by the cells. Considering this, Au cluster–BSA conjugates having very high concentrations of BSA ($\sim$50 mg ml^{-1}) [12] are not favorable for targeted delivery because of the dominant role of protein, leading to non-specific uptake by the cells. In this report, we address both these issues by using a combination of a green-chemical reducing agent, vitamin-C, and a low concentration of BSA for the synthesis of highly fluorescent Au NCs with bright red fluorescence in the NIR range and surface derivatized with molecular targeting ligands, namely folic acid (FA) for target-specific detection of cancer. To the best of our knowledge, this is the first report showing molecular-receptor-based targeted imaging of cancer using fluorescent Au nanoclusters (Au NCs) stabilized in BSA.

2. Experimental: materials and methods

2.1. Nanocluster synthesis

All reactions were performed in aqueous medium at room temperature. In a typical synthesis, 10 mM aqueous solution of $HAuCl_4$ (Spectrochem PVT Ltd, Mumbai) was reacted with $\sim$20 mg ml^{-1} BSA (Sigma Aldrich, USA) under vigorous stirring at 37 °C. To this solution of Au (I)–BSA complex, $\sim$1 μM total concentration of ascorbic acid was added drop-wise at a rate of $\sim$4 μl min^{-1} followed by the drop-wise addition of $\sim$1 M NaOH (Qualigens, India) to trigger the reduction of BSA-encapsulated Au precursor by ascorbic acid. This solution was continuously stirred at 37 °C for $\sim$6 h. During this period, the color of the colloid gradually changed, from transparent to dark yellowish brown and the red fluorescence emission indicated the nucleation of Au nanoclusters.

2.2. Bioconjugation of Au_n–BSA nanoclusters with folic acid (FA)

Au_n–BSA clusters were conjugated with folic acid (FA) using a zero-length cross-linker 1-ethyl-3-[3-dimethylaminopropyl] carbodiimide hydrochloride (EDC). FA was activated to become amine-reactive by linking with EDC. Typically,

~25 mg EDC (Sigma Aldrich, USA) was added to 10 mg of FA (Sigma Aldrich, USA) in 500 μl PBS (136.9 mM NaCl, 2.68 mM KCl, 8.1 mM Na_2HPO_4, 1.47 mM KH_2PO_4, pH 7.4). After 5 min of incubation at room temperature with probe sonication, the solution was added to 150 mg of Au–BSA NCs dissolved in 3 ml PBS. After 2 h of incubation at room temperature with stirring, the pH of the reaction mixture was adjusted to ~9 and promptly passed through a desalting column (Zeba Desalt Spin Columns provided by Thermo Scientific, India). Alkalization of the reaction mixture was necessary for the complete separation of free folate from the conjugate [15]. Successful conjugation of FA to Au–BSA clusters was confirmed by FTIR and UV–vis absorption spectroscopy. The conjugated clusters are hereafter referred to as Au–BSA–FA NCs.

2.3. Nanocluster characterization

The nanoclusters' size determination was done using a JEOL 3010 model transmission electron microscope. Atomic force microscopy (AFM), JEOL JSPM-5200, was also used to obtain the size and morphology of the colloidal samples spray-coated over an atomically flat mica substrate. The binding energy of Au–BSA and Au–BSA–FA NCs was determined by x-ray photoelectron spectroscopy which is an ESCA probe TPD system with integrated x-ray source. Fourier-transform infrared spectra of samples supported on KBr pellets were recorded using a Perkin Elmer Spectrum RX1 for evaluating the encapsulation of Au NCs by BSA and conjugation of FA with Au–BSA NCs. UV–vis absorption spectra of BSA, Au–BSA, FA and Au–BSA–FA NCs were recorded using a UV-1700 Pharma Spec UV–vis spectrophotometer. Concentration of BSA present in the final washed product was estimated from the standard linear curve. Luminescence emission and excitation spectra of Au–BSA–FA clusters, dissolved in aqueous solution, were recorded at room temperature, using a HORIBA JOBIN-YVON Fluoromax 4 spectrofluorometer with excitation and emission slits at 5 nm with appropriate filters for removing the second-order diffraction peaks. Near-infrared imaging of Au–BSA–FA NCs were recorded in cell-free phantom samples prepared by pelletizing lyophilized powder into circular discs of thickness ~10 mm and imaged using a Kodak *In vivo*-FX Multispectral Imaging Station. The samples were excited at 650 nm (±5 nm) and emission was recorded using the 700–750 nm band-pass emission filter at the detector side for 30 s integration time.

2.4. Fluorescence quantum efficiency

Fluorescence quantum efficiencies (QE) of Au–BSA and Au–BSA–FA NCs were measured by a comparative method as reported earlier [7]. The QE of a sample (QE_S) is derived from the equation $QE_S = (I_S \times QE_R)/I_R$, where I_S is the integrated emission intensity of the sample; QE_R and I_R are the QE and integrated emission intensity of the reference sample, respectively. For direct comparison with earlier reports, we used the same fluorescence reference sample, fluorescein (QE ~ 0.95), in our experiments. Optical densities of both the test sample and reference were adjusted to 0.1 at their corresponding excitation peak maximum, 569 nm for Au NCs and 480 nm for fluorescein. Optical density and fluorescence intensity were recorded under identical instrument settings. Since we used the same solvent (water) for both the test and reference samples, the correction factor for the refractive index of the solvent was found insignificant in the calculation. For each sample, the optical density was recorded using a UV-1700 Pharma Spec. UV–vis spectrophotometer and the corresponding photoluminescence spectrum was recorded using a HORIBA JOBIN-YVON Fluoromax 4 spectrofluorometer.

2.5. Cell line experiments

2.5.1. MTT cell viability assay. Primary endothelial cells are most suitable for toxicity analysis [16], because nanoparticles will be first encountered by the endothelial system after i.v. injection. Human umbilical vein endothelial cells (HUVEC) were isolated from umbilical veins of healthy volunteers, as per the protocol approved by the clinical ethics committee of the Institute. They were propagated for at least three population doublings before toxicity studies in Iscove's Modified Dulbecco's Medium containing 20% FBS and 50 IU ml^{-1} penicillin. FR^{+ve} oral carcinoma KB cells and FR^{-ve} lung cancer A549 cells were provided by the National Center for Cell Sciences, Pune, India. RPMI 1640 medium without and with FA (Sigma Aldrich, USA) were used for KB and A549, respectively. All the media were supplemented with 10% FBS (Gibco, USA) and 50 IU ml^{-1} penicillin (Gibco, USA) 50 IU ml^{-1} streptomycin (Gibco, USA). Cells were cultivated in the medium at 37 °C in a humidified environment of 5% CO_2. KB and A549 cells were trypsinized and seeded at a density of 5×10^3 (24 h study) into a 96-well tissue-culture plate. After 24 h old medium was discarded followed by replacement with media containing various concentrations (20, 80, 150, 300 and 500 $\mu g\,ml^{-1}$) of Au–BSA and Au–BSA–FA NCs. Negative controls were replaced with fresh 10% FBS-containing media whereas Triton X100 (1%) was added in the positive control. Triplicates were set up for each sample concentration, negative and positive control. After 24 h incubation the cultured cells were assayed for cell viability with MTT (Sigma). MTT stock solution (5 mg ml^{-1}) supplemented with 100 μl of serum-free medium was added into each well. After 4 h of incubation, the culture medium was removed and the purple crystals were dissolved in 110 μl of the solubilization buffer (10% Triton X100 and 0.1 N HCl in isopropanol). The optical density values at 570 nm were measured using the microplate reader (Biotex Power Wave XS Model).

2.5.2. Measurement of intracellular ROS by flow cytometry. Intracellular accumulation of reactive oxygen species (ROS) was determined with dichlorofluorescein-di-acetate (DCFH-dA, M/S Invitrogen). This nonfluorescent compound accumulates within cells upon de-acetylation. DCFH then reacts with ROS to form fluorescent 2,7-dichlorofluorescein (DCF). KB cells were trypsinized and seeded at a density of 2×10^5 cells/well into 6-well tissue-culture plates. After 12 h, old

medium was discarded followed by replacement with medium containing 500 μg ml^{-1} of Au–BSA–FA NCs. Negative controls were replaced with fresh 10% FBS-containing medium and 500 μg ml^{-1} H_2O_2 was added in the positive control. After 12 h of incubation at 37 °C, cells were washed with PBS (pH 7.4) three times and incubated with 30 μM of DCFH-dA (dissolved in 100% ethanol, filter sterilized) at 37 °C for 30 min. The cells were then harvested with trypsin. The intensity of fluorescence was detected by flow cytometry (BDFACSAria™ II) with an excitation filter of 488 nm and a band-pass emission filter of 530 ± 15 nm.

2.5.3. Cellular uptake studies by fluorescent microscopy. For FR-targeted cancer imaging, oral carcinoma KB cells and breast adenocarcinoma MCF-7 cells were up-regulated for the folate receptors by growing in folate-free RPMI 1640 medium at 37 °C with 5% CO_2 for 3 weeks. As negative controls, the FR^{-ve} cancer cell line A549 was cultivated under similar conditions in RPMI 1640 medium supplemented with 10% serum. Further, FR-depressed KB cells (FRd) were also used to confirm the FR-targeted delivery of QDs. For this, 100-fold molar excess of free FA was added to the cell suspension 10 min prior to the addition of Au–BSA–FA conjugates. For imaging study, cells were trypsinized and seeded on 13 mm glass cover slips placed inside 24-well tissue-culture plates at a seeding density of 1×10^3 cells/cover slip. After 23 h, the adherent cells were washed twice with PBS followed by replacement of media containing bare and FA-conjugated BSA encapsulated Au NCs with 1 mg ml^{-1} concentration and incubated for 2 h at 37 °C. Cells were then washed one time with PBS (300 μl/well), fixed with 2% paraformaldehyde for 20 min and mounted with the mounting medium. For DAPI staining of the nucleus ∼500 μl half diluted DAPI (Sigma Aldrich, India) from the main stock concentration of 500 μg ml^{-1} was incubated for 7–8 min with the cells. After PBS washing, the cover slips were mounted on glass slides with DPX mountant and the fixed cells were imaged on an Olympus BX-51 fluorescent microscope equipped with a color CCD camera (Model DP71) and 60× oil immersion objectives. NC fluorescence was detected using band-pass excitation and emission filters (BP 480–550 nm excitation, 590 nm emission and 570 nm dichromatic mirror).

2.5.4. Nanocluster uptake studies by spectrofluorimetry. Oral cancer cell, KB, breast cancer MCF-7 cells and lung cancer A549 cells from a confluent flask were seeded at a density of 1×10^6 cells per well in a 6-well plate. RPMI FA-free medium supplemented with 10% FBS and 50 IU ml^{-1} antibiotics was used for culturing the cells. After 24 h of incubation in a humidified atmosphere of 5% CO_2 at 37 °C old medium was discarded and new medium containing FA-conjugated and-unconjugated Au–BSA NCs were added. The cells were incubated in this medium for 4 h. Cells without any nanoconjugates and PBS were used as the controls. The cells were washed twice with PBS and trypsinized and a cell pellet was collected by centrifuging at 1500 rpm for 5 min. The cells were lysed with 10 μl cell-lyses buffer containing protease inhibitor. The lysed cells were re-suspended in 1 ml PBS and centrifuged at 10 000 rpm for 10 min. The supernatant was collected and the volume was made up to 3 ml using PBS. The integrated fluorescence emission intensity of both Au–BSA and Au–BSA–FA NCs from cell lysate were measured using a HORIBA JOBIN-YVON spectrofluorimeter. The relative emission intensities at 674 nm from KB, MCF-7 and A549 cell-lysate were plotted.

3. Results and discussion

3.1. Nanocluster synthesis

According to the main objective of this work, to prepare bioconjugated fluorescent Au_n nanoclusters (NCs) for receptor-targeted cancer imaging, the synthesis and bioconjugation protocols were optimized considering the following factors: (a) minimum use of cluster-stabilizing protein, BSA, which can cause non-specific uptake of Au clusters by the cells and (b) maintenance of cluster fluorescence over a wide range of pH from 4 to 9, which includes cell-culture pH ∼ 7.4 and intracellular lysosomal pH ∼ 4–5. Our initial cell targeting experiments with Au clusters containing high concentrations of BSA (50 mg ml^{-1}) [12] were found unsuccessful due to the non-specific uptake of nanoconjugates even without any folate targeting ligand on the surface of nanoclusters or control cells having no or depressed folate receptors on the membrane. Accordingly, in the subsequent experiments, we have reduced the BSA concentration to ∼20 mg ml^{-1} and a green-chemical reducing agent, ascorbic acid (vitamin-C), was used to trigger the formation of nanoclusters at a low BSA concentration. The role of ascorbic acid was evident from the fact that, with only 20 mg ml^{-1} BSA in the reaction medium, we have not observed the formation of Au clusters even after 24–48 h of reaction at 37 °C. In contrast, with the controlled addition of ascorbic acid, the colloidal system slowly turned from pale yellowish to brown after ∼3 h of reaction and started showing a typical bright fluorescence related to Au_{25} clusters [12]. Further, it was noted that, when the concentration of ascorbic acid exceeded 1 μM, or the rate of addition was accelerated >4 μl min^{-1}, uncontrolled precipitation occurred of larger Au nanoparticles of ∼20 nm showing surface plasmon resonance (absorbance) at ∼520 nm with no fluorescence. It is also to be mentioned that we had to readjust the concentration of the reducing agent within the range of 5–10%, when the source of supply of $HAuCl_4$ or BSA was changed, indicating the sensitivity of reaction parameters.

3.2. Characterization

3.2.1. Folic acid conjugation. Bioconjugation of FA with fluorescent Au clusters is an important aspect of the present work. Folic acid is a water-soluble vitamin (B_{11}) which is taken up by the cells through folate receptor (FR)-mediated endocytosis, namely potocytosis, which is especially important during the periods of rapid cell division and growth as in the case of cancer [17]. FR is a glycosylphosphatidylinositol (GPI)-anchored high-affinity membrane protein, over-expressed in a number of human tumors including ovarian cancer and squamous cell

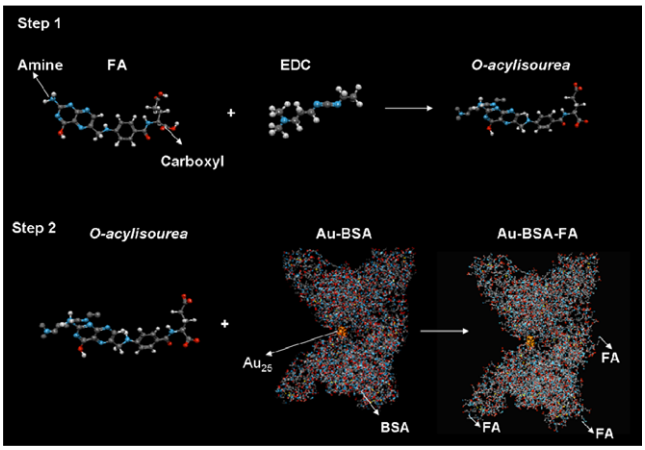

Figure 1. Bioconjugation scheme for BSA-stabilized Au cluster: step 1: FA is reacted with EDC to form an amine-reactive O-acylisourea intermediate. Step 2: O-acylisourea intermediate reacts with primary amines on the surface of BSA to form Au–BSA–FA conjugates.

carcinoma. The normal tissue distribution of the folate receptor is highly restricted, making it a useful marker for targeted drug delivery to tumors. FA retains its receptor binding affinity when covalently linked to the drug/contrast agent through its gamma-carboxyl group. FA-based targeting is attractive over antibodies because of its smaller size, lack of immunogenicity, ready availability, low cost and relatively easy bioconjugation chemistry [18–20]. Considering these aspects, we chose FA to conjugate with Au–BSA NCs for targeting the cancer cells that over-express FR, called FR^{+ve} cells. Since the molecular surface of BSA has several amine groups and FA has carboxylic groups, direct conjugation through amine–carboxylate linkage was possible. Figure 1 depicts the schematic diagram of the reaction sequence used for the bioconjugation reaction. First, FA is 'activated' into an amine-reactive succinimide ester using a well-known carbodiimide cross-linker (EDC) which reacts with a γ-COOH group of FA at pH 4.5, forming an amine-reactive O-acylisourea intermediate which readily reacts with primary amines in BSA at pH 7.4. One of the major challenges in this reaction sequence was to protect Au clusters from losing their cluster character due to the reaction of BSA with FA. The molecular nature of Au clusters having only a few tens of atoms makes its physico-chemical stability and properties highly sensitive to the surface ligand and hence the introduction of FA to the protective BSA shell can lead to changes in the cluster properties, such as fluorescence emission and binding energy. At the same time, an optimum concentration of FA was needed to achieve efficient cell targeting. Hence, a 'trade-off' between the stability of the Au core to cell targeting efficacy and fluorescence was achieved by optimizing the FA/BSA ratio to ∼0.02 (w/w). The minimum concentration of FA needed for effective cell targeting was empirically identified by varying the concentration ratio of FA/BSA (w/w) from 0.01 to 0.1. From the experimental results (fluorescence and cell targeting efficacy), the FA/BSA ratio of ∼0.02 (w/w) has been optimized and maintained for all Au–BSA–FA samples discussed hereafter, unless otherwise specified.

3.2.2. Atomic force microscopy and transmission electron microscopy of Au–BSA–FA conjugates. Atomic force microscopy (AFM) was used to image the morphology of Au–BSA–FA conjugates, formed by spray-coating of the colloidal sample as a thin film on an atomically flat mica substrate. Figure 2(a) shows the AFM image of Au–BSA–FA conjugates where the digitally enlarged part (figure 2(a), inset) shows relatively larger conjugates of size ∼8.5 nm, indicating the formation of nanoparticulates of Au–BSA–FA. Essentially, the sub-nanometer-sized molecular Au clusters are embedded within these self-assembled protein aggregates, but they retained the characteristic cluster fluorescence, as observed under the fluorescence microscopic imaging of the same film, shown in figure 2(b). Further, in TEM imaging (figure 2(c)) individual nanoclusters (marked by arrows) of size ∼1 nm were found distributed all throughout the imaging area. Relatively large (8 nm) aggregates of Au–BSA–FA conjugates (marked by circles) could also be seen.

3.2.3. X-ray photoelectron spectroscopy. X-ray photoemission spectra indicating the binding energy of the Au core of

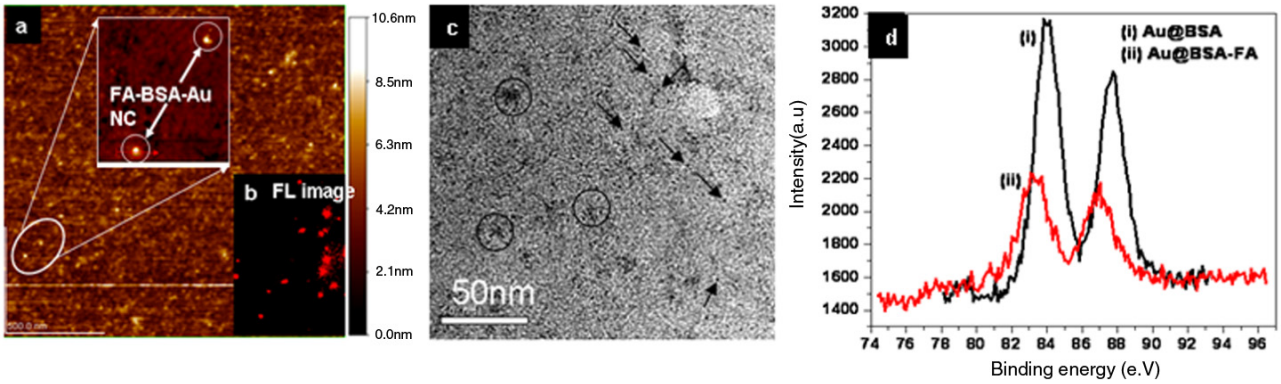

Figure 2. (a) AFM image of Au–BSA–FA cluster conjugates recorded from a film formed over atomically flat mica substrate, Inset: digitally enlarged image of relatively larger, spherical aggregates of size ∼8.5 nm, (b) fluorescent image of the aggregated clusters from the same film, (c) TEM image of nanoclusters; aggregates are marked by circles while separated Au–BSA–FA clusters are marked by arrows, (d) XPS data showing binding energy of Au–BSA and Au–BSA–FA.

the conjugates are shown in figure 2(d). The observed binding energy values for optimized conjugates show Au $4f_{7/2}$ ∼ 83.97 eV and Au $4f_{5/2}$ ∼ 87.768 eV, which correlate very well with the metallic Au (0) [25, 26]. However, it is interesting to note that, when conjugated with FA at a higher concentration of FA/BSA ⩾ 0.02, the XPS data exhibits a slight shift in the binding energy, indicating direct electron transfer from FA to Au core or changes in the BSA–Au ligand–core interactions. We considered this as the maximum limiting concentration of the targeting ligand FA, above which the core–ligand interactions leading to changes in the physicochemical characteristics of Au clusters occur. Although detailed XPS analysis will be needed to understand the exact nature of such interactions, for the practical purpose of cancer cell targeting, this unfavorable condition was avoided by maintaining the FA/BSA concentration well below 0.02 where the Au core retained its Au^0 metallic status together with good fluorescence efficiency, ∼5.7%, and cell targeting efficacy. Essentially, the XPS studies reveal the importance of understanding the core–ligand interactions while bioconjugating the nanocluster systems and the need to optimize ligand concentration for retaining the cluster properties.

3.2.4. Fourier-transform infrared spectroscopy. The bioconjugation scheme was analytically followed using Fourier-transform infrared (FTIR) spectroscopy. Figure 3 shows the FTIR spectrum of BSA, Au–BSA, FA and Au–BSA–FA NC conjugates, respectively. The characteristic amide I band of BSA can be seen at 1654 cm^{-1} as expected for a protein with a high proportion of α-helix. The band appearing at 1545.00 cm^{-1} can be attributed to strong primary amine scissoring, whereas the band centered at 3435.98 cm^{-1} can be attributed to primary amines. The band appearing at 2958.79 cm^{-1} corresponds to C–H vibration and the broad band at 701.65 cm^{-1} can be attributed to $-NH_2$ and $-NH$ wagging [21]. In the final conjugate of Au–BSA–FA NCs, all the characteristic vibrational modes associated with FA, such as C–H stretching at 2943.00 cm^{-1} and aromatic ring stretch of the pyridine and p-amino benzoic acid moieties in the range of 1476–1695 cm^{-1}, can be clearly seen. Peaks at 1336.00 and 912.00 cm^{-1} show the presence of aromatic C–H in-plane and out-of-plane bending, respectively [22]. The line broadening appearing over 1652–1350 cm^{-1} is indicative of the covalent linkage of FA with BSA.

3.2.5. UV–vis absorption spectroscopy. The synthesis and bioconjugation steps were also followed using UV–vis spectroscopy. The absorption spectra of BSA and Au–BSA NCs are shown in figure 4(a) while that of FA and Au–BSA–FA NC conjugates are depicted in figure 4(b), respectively. Au–BSA NCs show a prominent absorption at 280 nm which correlates with the classic absorbance of aromatic amino acids, mainly tryptophan and tyrosine [23]. The additional new absorbance seen over the 300–450 nm region can be attributed to the HOMO–LUMO electronic transition within Au clusters, which is not observed in the case of pure BSA. From the absorption spectra, the concentration of BSA is estimated to be ∼17.5 mg ml^{-1} in the final Au–BSA system formed by taking ∼20 mg ml^{-1} of BSA in solution. Accordingly, FA-conjugated samples with different FA to BSA ratios were prepared and a representative UV–vis data (figure 4(b)) of Au–BSA–FA with FA/BSA ratio of 0.02 (w/w) show the presence of characteristic absorption features of FA in the 250–280 and 320–400 nm ranges [24] with a distinct absorption hump at 320–400 nm (marked by the circle) which exemplifies the HOMO–LUMO transition of Au clusters embedded within the conjugates.

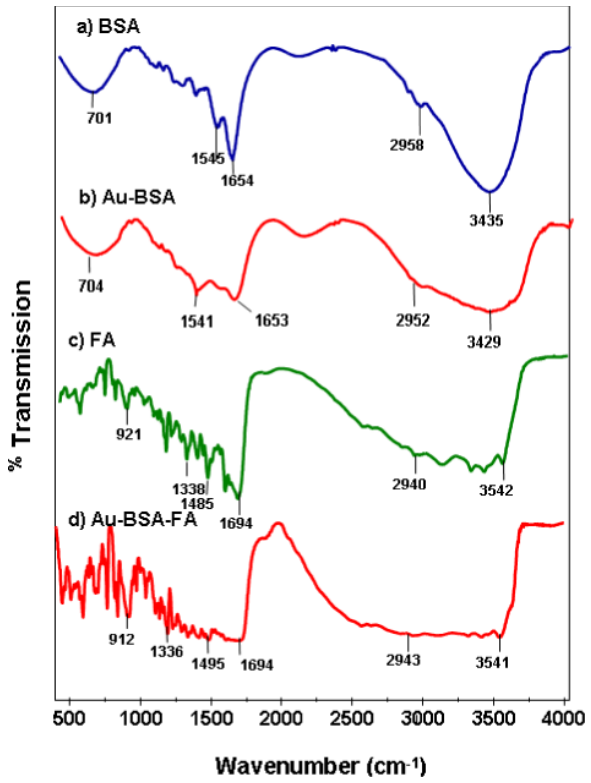

Figure 3. FTIR spectra of (a) BSA, (b) Au–BSA, (c) FA and (d) Au–BSA–FA samples, recorded in KBr-supported pellets. The characteristic vibration bands related to BSA and FA can be clearly seen in the final conjugates of Au–BSA–FA.

3.2.6. Photoluminescence properties. Photoluminescence excitation and emission spectra of Au–BSA–FA conjugates dissolved in water and recorded at room temperature are depicted in figure 5(a). The concentration of the conjugate is maintained at 1 mg ml^{-1}. The photoluminescence excitation spectrum recorded for red emission at 674 nm exhibited double maxima at 530 and 569 nm, which correlate well with the typical Au_{25} fluorescence related to HOMO–LUMO electronic transitions as reported earlier [12]. When excited using 530 or 569 nm light, the sample showed broad fluorescence spectra with a peak maximum at 674 nm, with the spectral edge extending to the near-infrared region (NIR) up to 800 nm. From the photoluminescence spectra, it is clearly evident that this fluorescence is characteristic of Au_{25} clusters and not Au_8, which gives blue fluorescence due to interband transitions [27]. The origin of photoluminescence from the Au NCs has been discussed by several authors using a solid-state model for the electronic structure and relaxation of

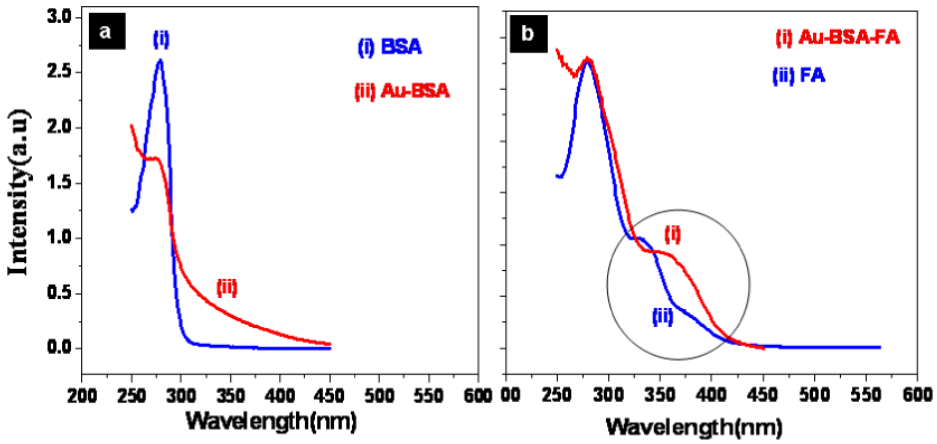

Figure 4. UV–vis absorption spectra of (a) BSA and Au–BSA, (b) FA and FA-conjugated Au–BSA. The region in the circle shows an additional absorption hump indicating the presence of Au clusters in Au–BSA–FA conjugates.

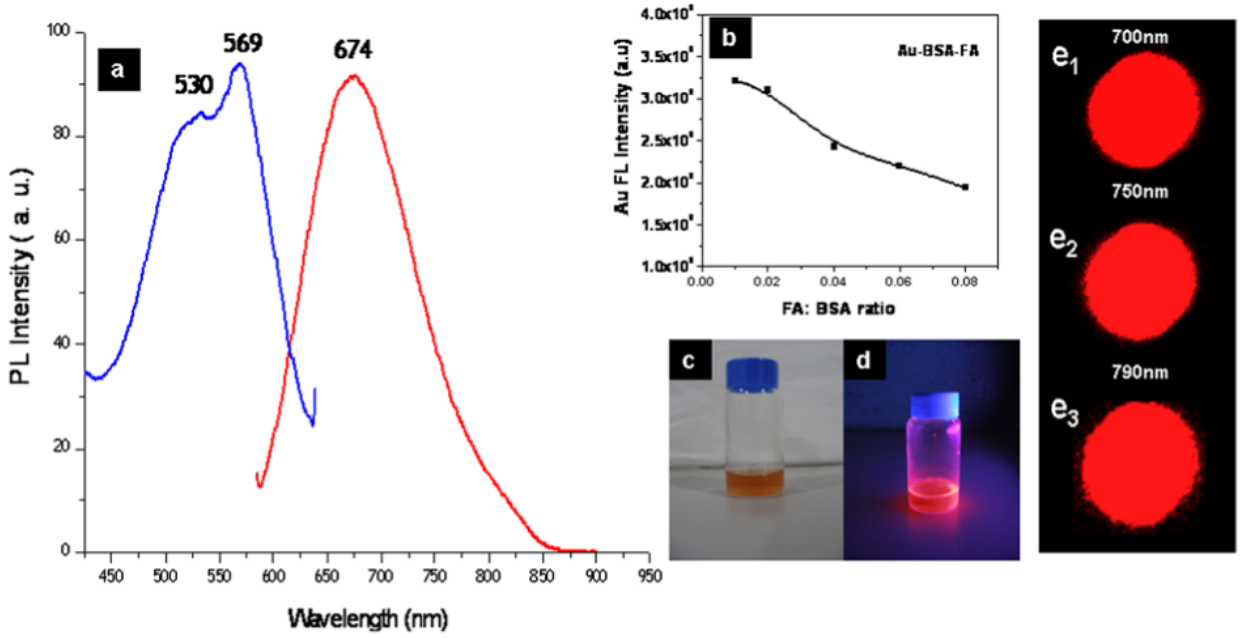

Figure 5. (a) Excitation and emission spectrum of Au clusters, (b) changes in the fluorescence intensity of Au clusters with increase in FA conjugation indicating core–ligand interactions, (c) photograph of Au–BSA NCs under white light illumination, (d) UV 365 nm excitation and (e_1)–(e_3) NIR imaging of phantom samples under 630 nm excitation and emission at 700 nm; 10 s integration; 750 nm, 1 s integration and 790 nm with 30 s integration time.

the clusters [8, 9, 28, 29]. In bulk phase, metals do not have energy bandgaps. However, for both semiconductor and (transition-) metal NPs, one interesting property is the appearance of an energy bandgap with decreasing particle dimensions [30]. Luminescence studies on neutral metal clusters show the observation of photoluminescence near 440 nm for <5 nm-sized gold particles after excitation at 230 nm. The origin of this photoluminescence was attributed to sp to d-band transitions which are high-energy transitions analogous to intraband transitions in bulk gold. It was expected that the photoluminescence mechanism for these NCs in the NIR range would involve low-energy transitions across the HOMO–LUMO gap as depicted (figure 6(b)). Recently, Whetten *et al* [7] and Murray *et al* [29] separately reported the observation of NIR to visible fluorescence from nanosized Au NPs of size <1.8 nm and interpreted the NIR emission is due to HOMO–LUMO electronic transition of lower energy than that of the d–sp interband transition whereas the visible emission was ascribed to the interband transitions between the filled $^5d_{10}$ band and the $^6sp_1$ conduction band.

Considering the specific objective of targeted cancer imaging using Au nanoclusters, our focus was to synthesize clusters showing bright and stable fluorescence in the NIR range, particularly after bioconjugation with the targeting ligand and delivery into intracellular regions, where the lysosomal pH (~4.5–5) may affect the cluster fluorescence. Under the present synthesis method, the Au–BSA conjugates have shown excellent fluorescence stability over a wide range

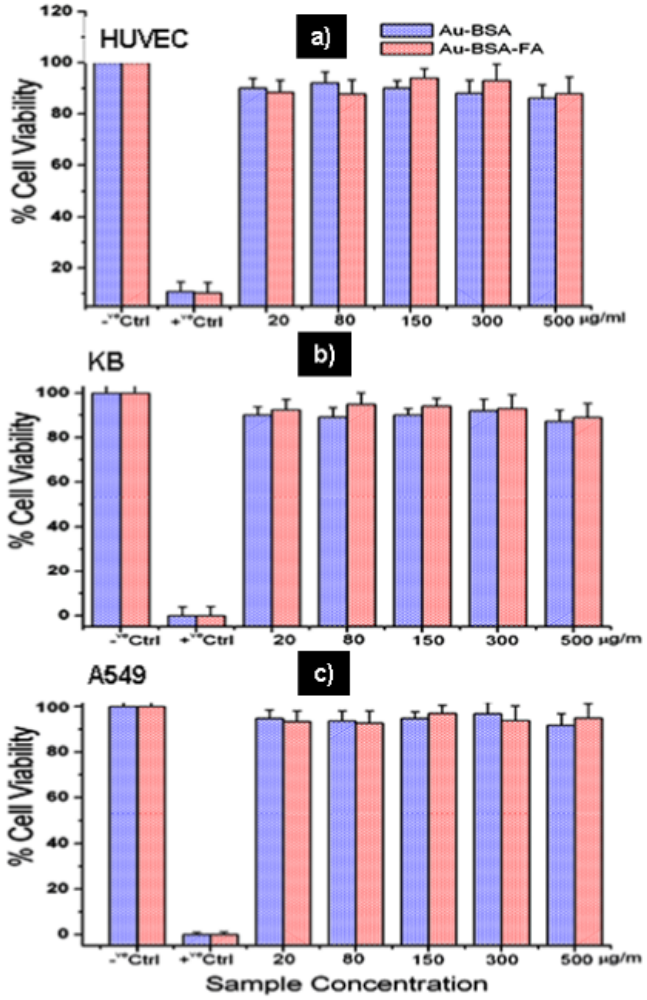

Figure 6. MTT cell viability assay on (a) primary HUVEC cells, (b) FR^{+ve} KB cells and (c) FR^{-ve} A549 cells in a 24 h study. Concentration used for both Au–BSA and Au–BSA–FA samples was 500 μg ml^{-1}, positive control: Triton X100, negative control: cells without nanoclusters.

of pH from 4 to 14. However, we have found that, during bioconjugation, with increasing FA concentration above the FA/BSA ratio >0.02, the fluorescence intensity of clusters gradually reduced, as shown in figure 5(b). Apparently, although BSA was acting as a strong stabilizing agent, the radiative transitions within the Au core were found to be affected due to FA conjugation. Similar observations were reported in thiol-protected Au clusters, $(Au)_nSG_m$, where the presence of ligands on the surface of Au NCs was found significantly influencing the electronic distribution [31–33]. This strongly suggests that the surface chemistry plays a vital role in determining the electronic energy structure and hence the fluorescence characteristics of Au NCs. This aspect was important for our investigations because it is quite probable that, during the receptor–ligand interaction or during the enzymatic activity within the cells, the clusters may lose their fluorescence due to the modification or cleavage of Au–BSA bonds. Considering these issues, and from the empirical observations, we have optimized the minimum concentration of the FA/BSA ratio that is needed to maintain better fluorescence efficiency and cell targeting capability as ∼0.02. At this ratio, the quantum efficiency (QE) of Au–BSA–FA was found ∼5.7% which is only marginally lower than ∼6.0% of unconjugated Au–BSA nanoclusters.

3.2.7. Phantom imaging at near-infrared region. For non-invasive *in vivo* fluorescent imaging, near-infrared (NIR) excitation and emission characteristics are an essential requirement, because of favorable tissue-optical properties in this range. Accordingly, we tested the possibility of imaging the bioconjugated Au clusters under an NIR window (700–800 nm) using a Kodak multispectral imaging station fitted with an NIR-intensified CCD camera. Figure 5(c) shows the white light image of the colloidal sample and figure 5(d) shows the fluorescence emission from the sample under UV excitation. The same sample was lyophilized and pelletized into phantom samples and imaged under three different NIR emission ranges. Figures 5 (e_1), (e_2) and (e_3), respectively, show images recorded using 700 ± 10 nm, 750 ± 10 nm and 790 ± 10 nm emission filters under 630 nm excitation. Integration time was kept at 10 s for 700 and 750 nm windows whereas 30 s was kept for the 790 nm window. In all three imaging conditions, the samples showed bright NIR fluorescence, suggesting that these fluorescent Au clusters can be a promising choice for *in vivo* imaging applications.

3.3. Cell line experiments

For the development of a contrast agent for biomedical imaging applications, one of the most important screening criteria is its toxicity effects on biological systems. This is particularly important for nanoparticles because of its comparable size with biomacromolecules such as proteins or enzymes, leading to enhanced interactions. Although several nanoparticulate systems such as QDs were proposed to be excellent materials for contrast imaging, they were later found unsuitable for *in vivo* use due to the toxicity associated with heavy metals [34]. Hence, we evaluated the cytotoxicity of Au–BSA and Au–BSA–FA NCs on human primary endothelial cells derived from the umbilical cord (HUVEC) as well as two cancer cell lines having different levels of folate receptor expression: FR^{+ve} squamous cell carcinoma (KB) and FR^{-ve} lung carcinoma A549.

3.3.1. MTT assay. Different concentrations (20–500 μg ml^{-1}) of Au–BSA and Au–BSA–FA NCs were treated with ∼5×10^3 cells for 24 h. Negative controls were replaced with fresh 10% FBS-containing media whereas Triton X100 (1%) was added to the positive control. Triplicates were set up for each sample concentrations as well as negative and positive controls. After 24 h of incubation, the cultured cells were assayed for cell viability with an MTT assay. The results are shown in figure 6. It is interesting to note that, even up to relatively high concentrations of ∼500 μg ml^{-1}, both primary and cancer cells did not show any kind of toxicity due to their interaction with nanoclusters. The cells remained ∼100% viable even after 24 h of incubation which indicates the non-cytotoxicity of Au NCs. We believe that the protective coat of BSA must be having a

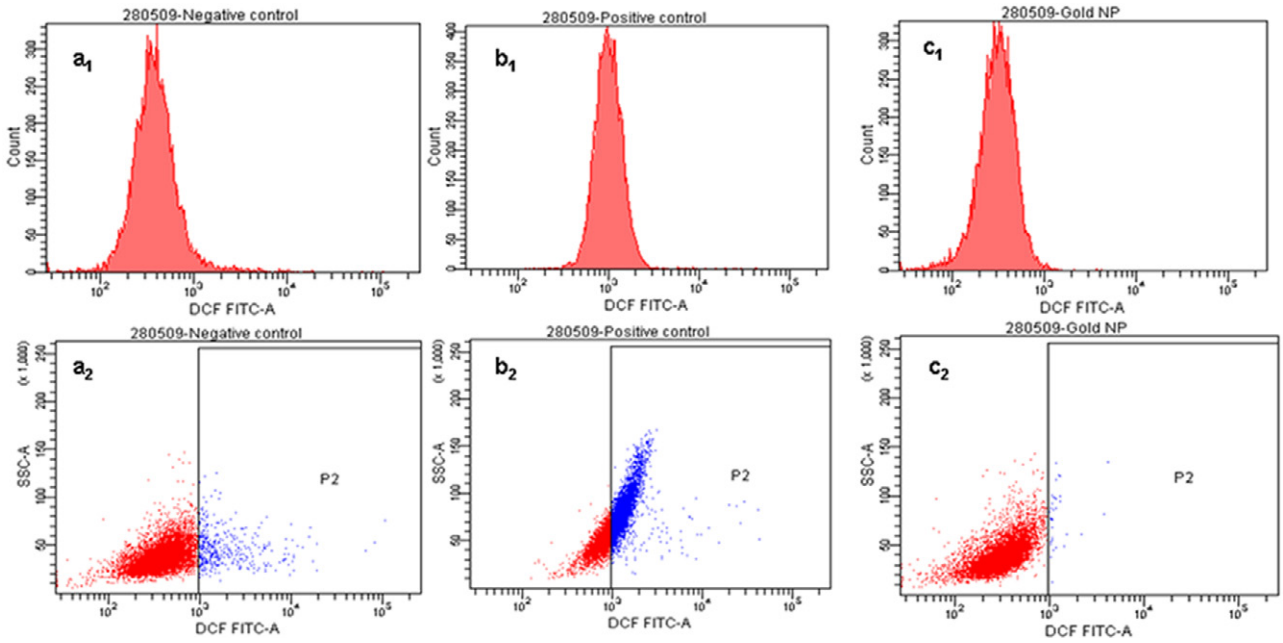

Figure 7. Intracellular ROS generation assay using dichlorofluorescein-di-acetate (DCFH-dA) shows the % of cells generating ROS in: (a_1)–(a_2) negative control cells without nanoclusters, (b_1)–(b_2) positive control of 500 μg ml^{-1} H_2O_2 and (c_1)–(c_2) cells treated with 500 μg ml^{-1} of Au–BSA–FA conjugates.

significant role in maintaining the bio-friendly nature of nanoclusters.

3.3.2. Intracellular ROS stress by flow cytometry. In addition to the MTT assay, which registers only the mitochondrial activity of cells or viability, we have also evaluated the reactive oxygen stress, if any, caused by the interaction of cells with Au NCs. Reactive oxygen species (ROS) was found to be one primary reason for toxicity by other nanomaterials [35]. Studies were carried out by monitoring the production of a fluorescent compound, 2,7-dichlorofluorescein (DCF), by the ROS species and counting those cells by flow cytometry. Untreated cells were used as negative control while cells with 500 μg ml of H_2O_2 were taken as positive control. Figures 7(a_1)–(a_2) depict the intracellular ROS concentration in untreated cells whereas figures 7(b_1)–(b_2) show ROS detected in the positive control (H_2O_2) which is ∼53.5% of the total cell count. In contrast, Au–BSA–FA conjugate-treated cells show practically no ROS stress in the total population as shown in figure 7(c_1)–(c_2). Most interestingly, the level of ROS from the cells treated with Au–BSA–FA was found to be even less (0.4%) than that of negative control (4.7%). This is possibly due to the fact that proteins and vitamins like folic acid can scavenge ROS formed in the cells [36, 37] and hence protect the cells. In effect, this implies that the Au–BSA–FA NCs are not only non-toxic but also protect the cells from other external stresses.

3.3.3. Receptor-specific detection of cancer using Au–BSA–FA cluster conjugates. The possibility of molecular-receptor-targeted optical detection of cancer using Au–BSA–FA conjugates was tested on FR^{+ve} KB cells with FR^{-ve} A549 cells, FR-depressed (FRd) KB cells and FR^{+ve} KB cells treated with unconjugated Au–BSA clusters as negative controls. Target specificity of FA-conjugated Au–BSA NCs was also tested in another cell line, breast adenocarcinoma MCF-7, which also over-expresses folate receptors but relatively less in comparison with oral cancer KB cells [39]. Prior to the targeting studies, in a separate set of experiments, we have characterized the folate expression level on KB cells using functional AFM imaging wherein FA-functionalized silicon tips were used to image the FR ligands from cell membranes [38]. The AFM images clearly showed significantly higher levels of FR expression on KB cells compared to the negative control and we used the same batch of cells for the present study. The concentration of nanoconjugates was maintained at 1.0 mg ml^{-1} in 250 μl of medium containing ∼1000 cells, incubated for 2–24 h, before fixing onto the glass slides for imaging. Figures 8(a_1)–(a_2) represent the bright-field and dark-field fluorescence images of FR^{-ve} A549 cells treated with Au–BSA–FA conjugates after 24 h of incubation (excitation: 480–550 nm, emission: 590 nm). It can be seen that, even after an extended duration of incubation with relatively high concentration of conjugates, no significant cellular uptake or staining of cell membrane could be seen. Some of the red-emitting clusters were found non-specifically located in the glass slide but not as a specific stain over the cell membrane. As another control, we used FR-depressed KB cells obtained by pre-treating the FR^{+ve} cells with 100 μM concentration of free FA. This way the FR receptors on cell membrane will be preoccupied with potocytosis and no active FR-mediated endocytosis will be possible on further treatment with the FA-conjugated clusters. This is evident from figures 8(b_1)–(b_2) that show the images of FRd KB cells incubated with Au–BSA–FA

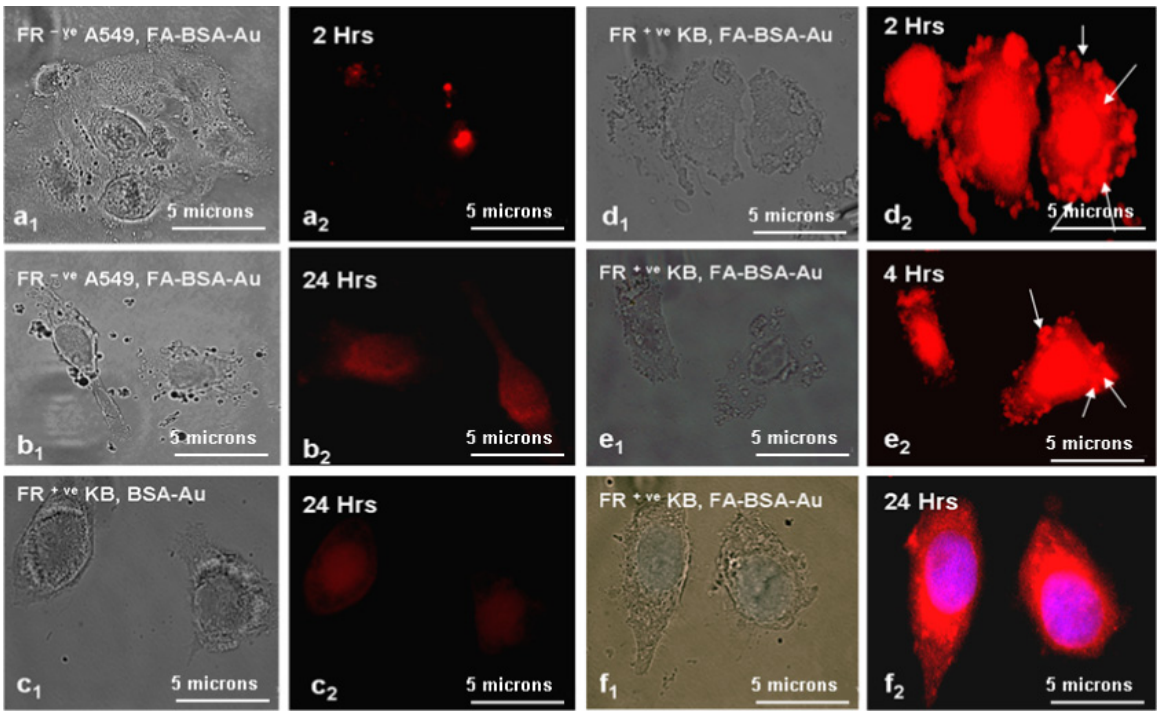

Figure 8. Fluorescent microscopic images showing interaction of Au–BSA–FA NCs with different types of cell lines: (a_1)–(a_2) FR^{-ve} lung carcinoma A549, (b_1)–(b_2) FR-depressed oral cell carcinoma, KB, (c_1)–(c_2) FR^{+ve} KB cells with unconjugated Au clusters, (d_1)–(d_2) FR^{+ve} KB cells with FA-conjugated Au clusters at 2 h, (e_1)–(e_2) 4 h and (f_1)–(f_2) 24 h of incubation.

for 24 h. There appeared to be no significant staining or cellular uptake suggesting no FA-mediated process and the non-specific uptake of Au–BSA–FA conjugates is insignificant even at relatively high concentration of conjugates (1 mg ml^{-1} for 1000 cells). This is further examined by treating the FR^{+ve} cells with unconjugated Au–BSA nanoclusters (figures 8(c_1)–(c_2)), which also showed no specific attachment of nanoclusters to the FR^{+ve} cell.

In contrast to the control experiments, the nature of interaction of FA-conjugated Au–BSA samples changed quite significantly when incubated with FR^{+ve} KB cells. In figures 8(d_1)–(d_2), KB cells treated with Au–BSA–FA at 2 h are shown. Interestingly, as early as 2 h, large numbers of red-emitting Au–BSA–FA conjugates were found specifically attaching to the cell membrane of FR^{+ve} KB cells. Relatively larger sized nano-aggregates, marked by white arrows, were accumulated mostly on the cell membrane while the solubilized clusters stain the whole cell, rendering a red fluorescent stain of the whole cell. With a longer incubation time of 4 h (figures 8(e_1)–(e_2)), the concentration of aggregated nanoclusters on the cell membrane was found reduced with an increase in fluorescence at the intracellular region. After 24 h, no aggregated nanoconjugates were seen on the cell membrane but found completely internalized in the cytosol. To differentiate the nucleus from cytosol, DAPI staining was carried out and the red emission (true-color imaging) from Au nanoclusters within the cytosol can be clearly seen. These results clearly suggest that the Au cluster conjugates were specifically taken up by the FR^{+ve} cells and the fluorescence intensity of internalized clusters remained intact, indicating the maintenance of cluster identity within the intracellular regions. In breast adenocarcinoma cells, MCF-7, the expression level of folate receptors is reported to be relatively low compared to that of KB cells [39]. We have tested corresponding relative changes, if any, in the FR-mediated uptake of nanoclusters in MCF-7 compared to KB cells by incubating the same concentration of FA-unconjugated and-conjugated Au–BSA NCs with MCF-7 and KB cells under identical culture conditions. In figure 9, it can be seen that, without any FA, the BSA–Au did not show any specific attachment to MCF-7 whereas FA-conjugated Au–BSA NCs showed enhanced uptake leading to red fluorescent staining of the cell membrane. The relative difference in the uptake was measured by spectrofluorimetric studies of red fluorescence from Au clusters present in the cell-lysates of KB, MCF-7 and A549 cells. Cells incubated without any nanoclusters and PBS were used as the controls. Prior to the experiment, the unattached nanoconjugates were washed out with PBS and cells were trypsinized and lysed. In figure 9(c), the emission intensity at 674 nm of Au–BSA–FA NCs was found higher in the case of KB cell-lysate. MCF-7 cell-lysate showed relatively less emission intensity compared to that of KB, but higher than that of A549. This result further confirms that the Au–BSA–FA conjugates were taken up by KB and MCF cells through FR-mediated endocytosis and there were relative changes in the uptake due to varied expression levels of the receptor. In effect, this study clearly demonstrates that the fluorescent Au nanoclusters can be successfully used for molecular-receptor-specific detection of cancer, at the single cell level, by optical imaging. Considering the near-infrared emission property and non-toxicity, the Au-nanocluster-based nanobioprobes will be

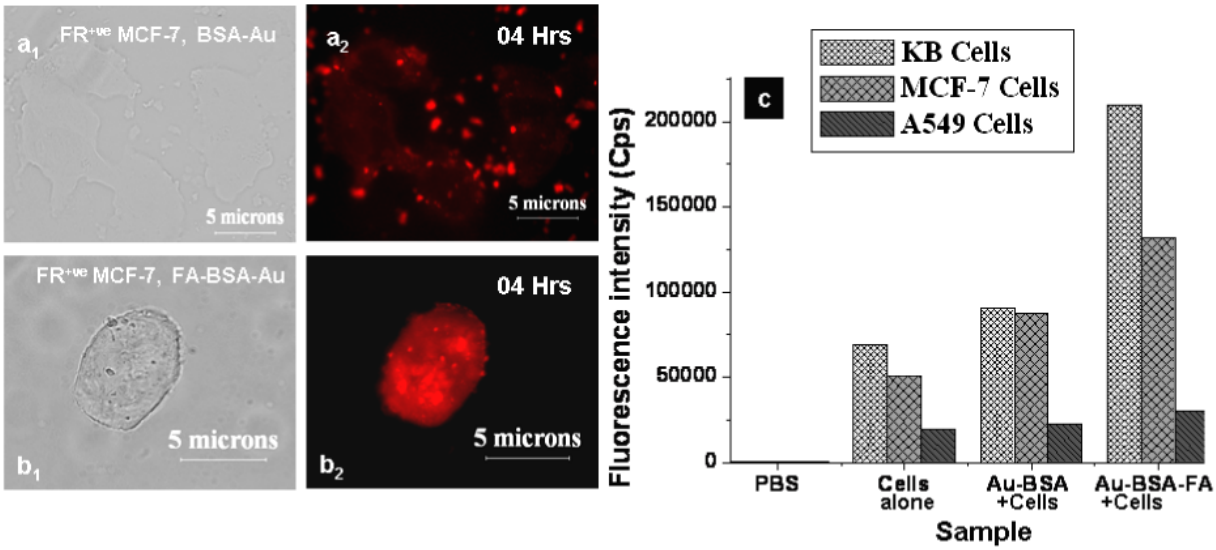

Figure 9. Fluorescent microscopic images showing interaction of Au–BSA NCs with MCF-7 cells: (a_1)–(a_2) unconjugated Au–BSA NCs treated with MCF-7 cells for an incubation period of 4 h, (b_1)–(b_2) Au–BSA–FA NCs treated with MCF-7 cells for 4 h, (c) integrated fluorescence intensity recorded from cell-lysate after treating with FA-conjugated Au–BSA NCs in KB, MCF-7 and A549 cells.

a better alternative to luminescent quantum dots for *in vivo* applications.

4. Conclusion

In summary, a novel bio-friendly fluorescent Au-cluster-based conjugate capable of specifically targeting molecular receptors on cancer cell membranes is presented. Aqueous colloidal formulations of albumin-protein-capped Au NCs of ∼25 atoms showing characteristic NIR fluorescence (600–800 nm) were synthesized using a simple green-chemical method and conjugated with a cancer targeting ligand, folic acid. The quantum efficiency of Au–BSA clusters was found to be ∼6%, with marginal reduction after folic acid conjugation as 5.7%. The concentration of FA and Au–BSA were optimized by considering a trade-off between the maintenance of bright fluorescence together with effective cancer targeting ability and minimum non-specific cellular uptake. The Au clusters showed broad fluorescence covering the NIR range, making it possible to image the clusters under 700–800 nm range where the tissue blood optical properties are highly favorable for biomedical imaging. The cytotoxicity studies using cell viability and ROS analysis suggested that Au NCs are non-toxic with no adverse effect on cell viability; rather, the residual ROS within the untreated cells disappeared after the nanocluster treatment, probably due to the free radical scavenging effect of the folic acid–protein combination. The molecular-receptor-targeted cancer detection using Au–BSA–FA conjugates was demonstrated using FR^{+ve} nasopharyngeal carcinoma cells, KB, wherein the nanoclusters specifically detect the KB cells while leaving the FR^{-ve} and FR-depressed control cells unstained. In the case of FA-conjugated samples, the membrane bound clusters were found internalized in a time-dependent manner suggesting FR-mediated endocytosis. The nanoclusters were also found maintaining its bright fluorescence after internalization into cytosol. The bio-friendly nature, near-infrared fluorescence and receptor specific cancer-targeting ability of Au clusters makes them an ideal candidate for optical-imaging-based cancer detection.

Acknowledgments

MK is grateful for financial support from the Department of Biotechnology (DBT), Government of India through RNAi program grant no. BT/PR10716/AGR/36/603/2008 and 'Nanotoxicology and Nanomedicine' program grant no. BT/PR9357/NNT/28/104/2007.

References

[1] Chan W C W, Maxwell D J, Gao X, Bailey R E, Han M and Nie S 2002 *Curr. Opin. Biotechnol.* **13** 40–6
[2] Haick H 2007 *J. Phys. D: Appl. Phys.* **40** 7173–86
[3] Huang X, Jain P K, El-Sayed I H and El-Sayed M A 2007 *Nanomedicine* **25** 681–93
[4] Alivisatos A P 1996 *Science* **271** 933–7
[5] Han M, Gao X, Su J Z and Nie S 2001 *Nat. Biotechnol.* **19** 631–5
[6] Weibo C, Andrew R H, Li Z-B and Chen X Y 2007 *Nanoscale Res. Lett.* **2** 265–81
[7] Link S, Beeby A, FitzGerald S, El-Sayed M A, Schaaff T G and Whetten R L 2002 *J. Phys. Chem.* B **106** 3410–5
[8] Negishi Y, Takasugi Y, Sato S, Yao H, Kimura K and Tsukuda T 2004 *J. Am. Chem. Soc.* **126** 6518–9
[9] Shichibu Y, Negishi Y, Tsunoyama H, Kanehara M, Teranishi T and Tsukuda T 2007 *Small* **3** 835
[10] Shiraishi Y, Arakawa D and Toshima N 2002 *Eur. Phys.* J **8** 377–83
[11] Singh S and Nalwa H S 2007 *J. Nanosci. Nanotechnol.* **7** 3048–70
[12] Xie J, Zheng Y and Ying J Y 2009 *J. Am. Chem. Soc.* **131** 888–9

[13] Jonas A and Weber G 1971 *Biochemistry* **10** 1335–9
[14] Lin C-A J *et al* 2009 *ACS Nano* **3** 395–401
[15] Lee R J, Wang S and Low P S 1996 *Biochim. Biophys. Acta* **1312** 237–42
[16] Jain S A, Rajwade J M and Paknikar K M 2009 *Toxicol. Appl. Pharmacol.* **236** 310–8
[17] Anderson R G, Kamen B A, Rothberg K G and Lacey S W 1992 *Science* **255** 410–1
[18] Antony A C 1992 *Blood* **79** 2807–10
[19] Setua S, Menon D, Asok A, Nair S and Koyakutty M 2010 *Biomaterials* **31** 714–29
[20] Manzoor K, Johny S, Thomas D, Setua S, Menon D and Nair S 2009 *Nanotechnology* **20** 065102
[21] Surewicz W K, Mantsch H H and Chapman D 1993 *Biochemistry* **32** 389–94
[22] Mohapatra S *et al* 2007 *Nanotechnology* **18** 385102
[23] Upstone S L 2000 *Encyclopedia of Analytical Chemistry* (Chichester: John Wiley & Sons Ltd) pp 1699–714
[24] Bossche D V, Van den Bossche J and Sherman D M 2006 *Bioconjug. Chem.* **17** 603–9
[25] Anthony M T and Seah M P 1984 *Surf. Interface Anal.* **6** 95
[26] Thomas T D and Weightman P 1986 *Phys. Rev.* B **33** 5406
[27] Zhang J Z 1997 *Acc. Chem. Res.* **30** 423–9
[28] Bigioni T P, Whetten R L and Dag O 2000 *J. Phys. Chem.* B **104** 6983–6
[29] Huang T and Murray R W 2001 *J. Phys. Chem.* B **105** 12498–502
[30] Negishi Y, Nobusada K and Tsukuda T 2005 *J. Am. Chem. Soc.* **127** 5261–70
[31] Shibu E S, Habeeb Muhammed M A, Tsukuda T and Pradeep T 2008 *J. Phys. Chem.* C **112** 12168–76
[32] Shibu E S, Radha B, Verma P K, Bhyrappa P, Kulkarni G U, Pal S K and Pradeep T 2009 *ACS Appl. Mater. Interfaces* **1** 2199–210
[33] Habeeb Muhammed M A, Verma P K, Pal S K, ArunKumar R C, Paul S, Omkumar R V and Pradeep T 2009 *Chem.—Eur. J.* **15** 10110–20
[34] Park E J and Park K 2008 *Toxicol. Lett.* **184** 18–25
[35] Park E-J, Yi J, Chung K-H, Ryu D-Y, Choi J and Park K 2008 *Toxicol. Lett.* **180** 222–9
[36] Roche M, Rondeau P, Singh N, Tarnus E and Bourdon E 2008 *FEBS Lett.* **582** 1783–7
[37] Armstrong J, Rajasekaran M, Hellstrom W J and Sikka S C 1998 *J. Androl.* **19** 412–9
[38] Girish C M, Binulal N S, Anitha V C, Nair S, Mony U and Prasanth R 2009 *Appl. Phys. Lett.* **95** 223703
[39] Sonvico F, Dubernet C, Marsaud V, Appel M, Chacun H, Stella B, Renoir M, Colombo P and Couvreur P 2005 *J. Drug Deliv. Sci. Technol.* **15** 407–10